Tissue refractometry using Hilbert phase microscopy

Niyom Lue,[1,3] Joerg Bewersdorf,[2] Mark D. Lessard,[2] Kamran Badizadegan,[1] Ramachandra R. Dasari,[1] Michael S. Feld,[1] and Gabriel Popescu[1,4,*]

[1]*G. R. Harrison Spectroscopy Laboratory, Massachusetts Institute of Technology, Cambridge, Massachusetts 02139, USA*

[2]*Institute for Molecular Biophysics, The Jackson Laboratory, Bar Harbor, Maine 04609, USA*

[3]*Department of Biomedical Engineering and Biotechnology, Multi-campus, University of Massachusetts, Boston, Massachusetts 02125, USA*

[4]*Present address, Quantitative Light Imaging Laboratory, Department of Electrical and Computer Engineering, Beckman Institute for Advanced Science and Technology, University of Illinois at Urbana-Champaign, Urbana, Illinois 61801, USA*

**Corresponding author: gpopescu@uiuc.edu*

Received September 28, 2007; accepted October 30, 2007;
posted November 12, 2007 (Doc. ID 88045); published December 10, 2007

We present, for the first time to our knowledge, quantitative phase images associated with unstained 5 μm thick tissue slices of mouse brain, spleen, and liver. The refractive properties of the tissue are retrieved in terms of the average refractive index and its spatial variation. We find that the average refractive index varies significantly with tissue type, such that the brain is characterized by the lowest value and the liver by the highest. The spatial power spectra of the phase images reveal power law behavior with different exponents for each tissue type. This approach opens a new possibility for stain-free characterization of tissues, where the diagnostic power is provided by the intrinsic refractive properties of the biological structure. We present results obtained for liver tissue affected by a lysosomal storage disease and show that our technique can quantify structural changes during this disease development.

OCIS codes: 170.6935, 180.3170.

The light scattering by tissues is fully determined by the three-dimensional refractive index distribution associated with the biological structure [1–4] On the other hand, the refractive properties of tissues reflect their structural organization, which can be used as an intrinsic marker for disease. However, due to its inhomogeneous distribution in all three dimensions, the tissue refractive index is extremely difficult to measure directly. Highly scattering tissue has been characterized in terms of an average refractive index by optical coherence tomography [5] and, more recently, total internal reflection [6]. Recently, we applied quantitative phase imaging to live cells flowing in microfluidic devices, which provides a high-throughput method for cytorefractometry [7].

In this Letter, we present a direct method for measuring the refractive index of biological tissues. The method extends, for the first time to our knowledge, the concept of quantitative phase imaging [8–12] to unstained tissue sections that are relevant for pathology and can be characterized as transparent, i.e., weakly absorbing and scattering objects. To measure these optical path-length maps, we employ Hilbert phase microscopy (HPM), which was developed in our laboratory for measuring quantitative phase images of cells with high lateral resolution and low noise [9,10].

To demonstrate the capability of our technique for quantifying the refractive properties of pathology tissue slices, we used samples prepared from three different mouse organs: brain, spleen, and liver. The tissue removed from the animal was fixed in 4% paraformaldehyde mixed with 1× phosphate-buffered saline (PBS). The 5 μm sections were obtained by using the Thermo Shandon Cryotome FSE cryostat and subsequently mounted on a glass slide in PBS.

Figure 1 shows examples of quantitative phase images of tissue slices from all sample groups, brain (a–c), spleen (d–f), and liver (g–j). The bright field images of these samples are shown for each group (a, d, g). It can be seen that these intensity maps of the tissue slices lack contrast and cannot reveal quantitative information about the structure. By contrast, the HPM images (b, e, i) uncover the architecture of the tissue and the spatial distribution of its optical properties. The quantitative phase images reflect the nonaqueous content of the sample [13]. This ability to quantify the dry content of biological samples without staining is a remarkable feature of quantitative phase imaging [14,15] and is not attainable with current optical microscopes. The phase images of the tissue from different organs appear qualitatively different. To quantify the spatially averaged properties of the tissue, we calculated the phase histogram associated with each HPM image. As illustrated in Figs. 1c, 1f, and 1j these histograms are clearly bimodal, with the first and second peaks due to the phase shifts of the background (PBS) and tissue, respectively. The difference, $\bar{\phi}$, between the mean values of the two distributions provides information about the average tissue refractive index, as $\bar{n}=(\bar{\phi}/2\pi)(\lambda/h)+n_{\mathrm{PBS}}$, where $h=5$ μm is the thickness and $n_{\mathrm{PBS}}=1.337$ is the refractive index of the embedding PBS. Our measurements employed ten HPM images for brain, eight for spleen, and seven for liver, with each image consisting of 640×480 pixels.

Figure 2a summarizes the results obtained in terms of $\bar{n}$ for the three sample groups. As illustrated in Fig. 2a, there are significant differences between

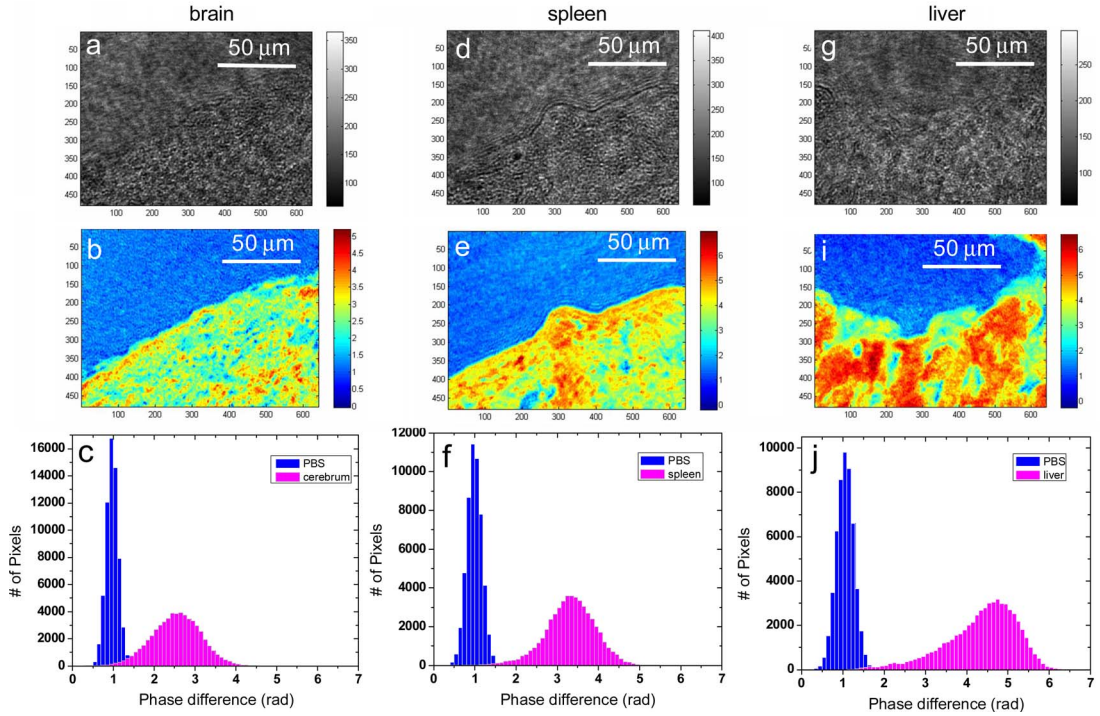

Fig. 1. (Color online) Examples of quantitative phase imaging studies of tissues slices: a–c, brain; d–f, spleen; g–j, liver. Row 1 shows the bright field images, row 2 the HPM images (color bars represent phase in radians), and row 3 the corresponding histogram of the phase shifts in row 2.

the refractive indices for the different tissues, with brain having the lowest and liver the highest values. These results can be explained by considering the high water content of the brain tissue, which determines a lower refractive index relative to the spleen and liver. To investigate the spatial organization of the tissue structure, we calculated the one-dimensional spatial power spectrum of the phase distribution $\phi(x)$ as

$$P(q) \propto \left\langle \left| \int \phi(x) e^{-i2\pi qx} \mathrm{d}x \right|^2 \right\rangle, \qquad (1)$$

where q is the spatial frequency and the angular brackets denote ensemble averaging over at least 50 profiles in each of the N tissue slices per group. Figures 2b–2d show the results in terms of the spatial power spectra for the three tissue types. The diffraction-limited resolution explains the drop at high spatial frequencies. Over a significant portion of the spatial frequencies, roughly $q \in (0.06, 0.6)\ \mu\mathrm{m}^{-1}$, the spectra show a power law behavior, as indicated by the linear trend of the log–log plots. The fit with this simple functional dependence can provide information about tissue architecture, as has been observed previously by using other microscopy techniques [16,17]. The exponents measured for these power law dependencies are shown in Fig. 2e. The differences among these three groups indicate the specific structural organization, i.e., "packaging" of the biological matter. It has been recently shown that the exponents of such power laws can be used to distinguish between normal and diseased tissues [18]. Figure 2f summarizes the results of both the

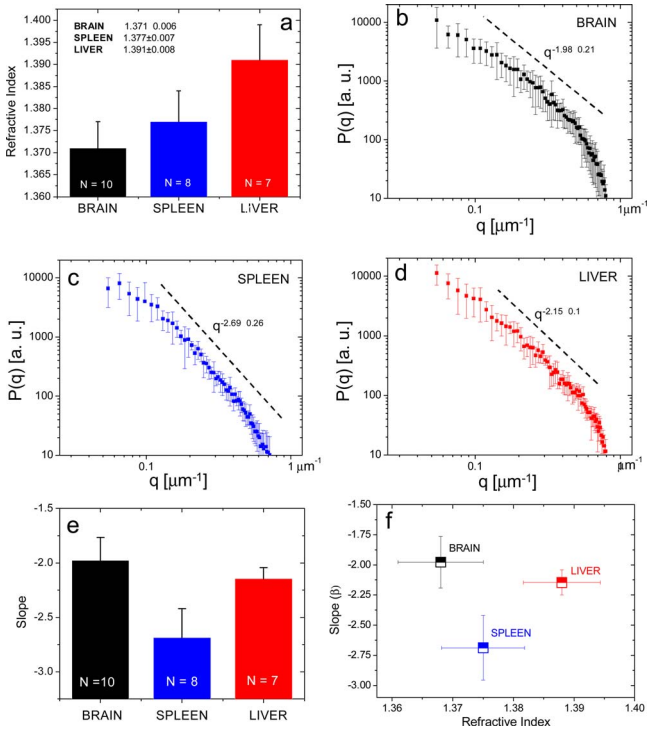

Fig. 2. (Color online) a, Average refractive index for the three sample groups, as indicated. The error bars indicate the sample-to-sample variation (N samples per group, as shown). b–d, One-dimensional power spectra for the three tissue types, as indicated. Dashed lines, power law functions of corresponding exponents. e, Power law exponents (slopes) for each sample group. The error bars indicate sample-to-sample variations (N samples per group with at least 50 profiles analyzed per sample). f, Exponent versus refractive index n for the three sample types. The corresponding error bars are indicated.

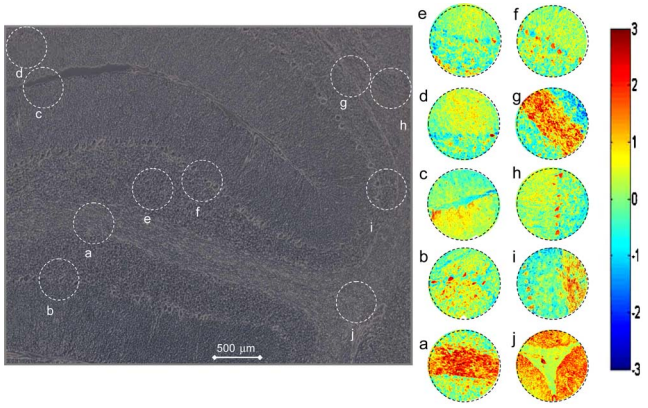

Fig. 3. (Color online) HPM images from various regions of a mouse cerebellum: a, area of white matter between areas of the granular layer; b, top to bottom, granular layer, Purkinje cell layer, molecular layer; c, areas of molecular layer on either side of a fissure between two cerebellar lobules; d, molecular layer; e, granular layer; f, top to bottom, molecular layer, Purkinje cell layer, granular layer; g, similar to a; h, circle in grayscale picture is different than the color picture; i, left to right, molecular layer, Purkinje cell layer, granular layer, white matter; j, white matter. The common color bar indicates phase shift in radians.

exponent and average refractive index, where the three sample groups appear well separated.

To better understand the large sample-to-sample variation within each tissue type shown in Fig. 2, we performed HPM imaging of brain tissue slices over large areas. Figure 3 illustrates the results on a large area of mouse cerebellum, shown as a bright field image (in gray scale). The HPM images corresponding to various regions in the cerebellum reveal the variability of the tissue properties.

To demonstrate the capability of our technique for disease diagnosis, we imaged mouse liver tissue affected by a particular type of lysosomal storage disease (LSD), referred to as Mucopolysaccharidosis Type VII, or Sly Syndrome [19]. In this LSD, due to malfunctioning of lysosomes (a type of cell organelles), long sugar chains are abnormally accumulated in the cell instead of being broken into smaller groups. As shown in Fig. 4, the progression of this disease in a mouse model can be easily observed by HPM imaging. Interestingly, we found that the average phase shift associated with the tissue does not vary significantly with disease. However, the pathlength standard deviation notably increases with the disease progression.

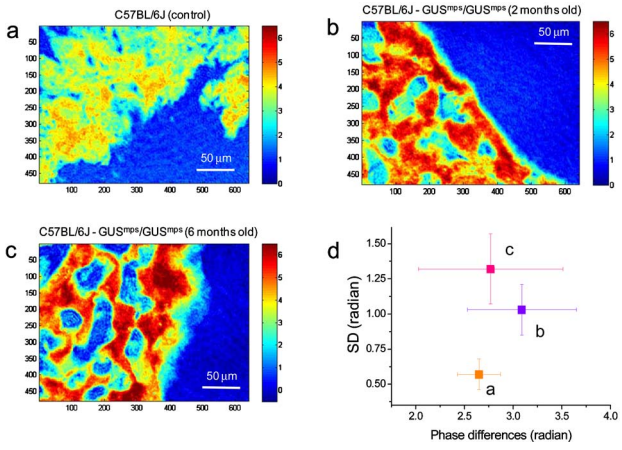

Fig. 4. (Color online) HPM images of liver tissue from LSD mouse model tissue. a, Normal control (C57BL/6J mouse); b, two-month-old diseased mouse (C57BL/6J-Gus^{mps}/Gus^{mps}); c, six-month-old diseased mouse (B6 C57BL/6J-Gus^{mps}/Gus^{mps}); d, phase standard deviation (SD) versus phase difference for the three tissue groups.

In summary, we presented quantitative phase images of tissue slices obtained by Hilbert phase microscopy. This approach can provide a powerful method for characterizing structural organization of healthy and diseased tissues, without the staining process that is currently used in standard histopathology.

References

1. V. Backman, M. B. Wallace, L. T. Perelman, J. T. Arendt, R. Gurjar, M. G. Muller, Q. Zhang, G. Zonios, E. Kline, J. A. McGilligan, S. Shapshay, T. Valdez, K. Badizadegan, J. M. Crawford, M. Fitzmaurice, S. Kabani, H. S. Levin, M. Seiler, R. R. Dasari, I. Itzkan, J. Van Dam, and M. S. Feld, Nature **406**, 35 (2000).
2. R. Drezek, A. Dunn, and R. Richards-Kortum, Appl. Opt. **38**, 3651 (1999).
3. J. R. Mourant, M. Canpolat, C. Brocker, O. Esponda-Ramos, T. M. Johnson, A. Matanock, K. Stetter, and J. P. Freyer, J. Biomed. Opt. **5**, 131 (2000).
4. V. V. Tuchin, *Tissue Optics* (SPIE, 2000).
5. G. J. Tearney, M. E. Brezinski, J. F. Southern, B. E. Bouma, M. R. Hee, and J. G. Fujimoto, Opt. Lett. **20**, 2258 (1995).
6. J. C. Lai, Z. H. Li, C. Y. Wang, and A. Z. He, Appl. Opt. **44**, 1845 (2005).
7. N. Lue, G. Popescu, T. Ikeda, R. R. Dasari, K. Badizadegan, and M. S. Feld, Opt. Lett. **31**, 2759 (2006).
8. G. Popescu, L. P. Deflores, J. C. Vaughan, K. Badizadegan, H. Iwai, R. R. Dasari, and M. S. Feld, Opt. Lett. **29**, 2503 (2004).
9. T. Ikeda, G. Popescu, R. R. Dasari, and M. S. Feld, Opt. Lett. **30**, 1165 (2005).
10. G. Popescu, T. Ikeda, C. A. Best, K. Badizadegan, R. R. Dasari, and M. S. Feld, J. Biomed. Opt. **10**, 060503 (2005).
11. Y. K. Park, G. Popescu, K. Badizadegan, R. R. Dasari, and M. S. Feld, Opt. Express **14**, 8263 (2006).
12. G. Popescu, T. Ikeda, R. R. Dasari, and M. S. Feld, Opt. Lett. **31**, 775 (2006).
13. G. A. Dunn and D. Zicha, J. Cell. Sci. **108**, 1239 (1995).
14. H. G. Davies and M. H. F. Wilkins, Nature **161**, 541 (1952).
15. R. Baber, Nature **169**, 366 (1952).
16. J. M. Schmitt and G. Kumar, Opt. Lett. **21**, 1310 (1996).
17. A. J. Einstein, H. S. Wu, and J. Gil, Phys. Rev. Lett. **80**, 397 (1998).
18. M. Hunter, V. Backman, G. Popescu, M. Kalashnikov, C. W. Boone, A. Wax, G. Venkatesh, K. Badizadegan, G. D. Stoner, and M. S. Feld, Phys. Rev. Lett. **97**, 138102 (2006).
19. E. H. Birkenmeier, M. T. Davisson, W. G. Beamer, R. E. Ganschow, C. A. Vogler, B. Gwynn, K. A. Lyford, L. M. Maltais, and C. J. Wawrzyniak, J. Clin. Invest. **83**, 1258 (1989).